Stochastic Models of Blood Vessel Growth

Luis L. Bonilla(✉), Manuel Carretero, and Filippo Terragni

G. Millan Institute, Department of Materials Science and Engineering,
Universidad Carlos III de Madrid, Leganés, Spain
bonilla@ing.uc3m.es,
{manuel.carretero,filippo.terragni}@uc3m.es

Abstract. Angiogenesis is a complex multiscale process by which diffusing vessel endothelial growth factors induce sprouting of blood vessels that carry oxygen and nutrients to hypoxic tissue. There is strong coupling between the kinetic parameters of the relevant branching - growth - anastomosis stochastic processes of the capillary network, at the microscale, and the family of interacting underlying biochemical fields, at the macroscale. A hybrid mesoscale tip cell model involves stochastic branching, fusion (anastomosis) and extension of active vessel tip cells with reaction-diffusion growth factor fields. Anastomosis prevents indefinite proliferation of active vessel tips, precludes a self-averaging stochastic process and ensures that a deterministic description of the density of active tips holds only for ensemble averages over replicas of the stochastic process. Evolution of active tips from a primary vessel to a hypoxic region adopts the form of an advancing soliton that can be characterized by ordinary differential equations for its position, velocity and a size parameter. A short review of other angiogenesis models and possible implications of our work is also given.

Keywords: Angiogenesis · Active vessel tip model · Stochastic differential equations · Reinforced random walk · Branching process · History-dependent killing process · Cellular Potts models · Integrodifferential equation for active tip density

1 Introduction

The growth of blood vessels out of a primary vessel or *angiogenesis* is a complex multiscale process responsible for organ growth and regeneration, tissue repair, wound healing and many other natural operations in living beings [1–5]. Angiogenesis is triggered by lack of oxygen (hypoxia) experienced by cells in some tissue. Such cells secrete growth factors that diffuse and reach a nearby primary blood vessel. In response, the vessel wall opens and issues endothelial cells that move towards the hypoxic region, build capillaries and bring blood, oxygen and

G. Giacomin et al. (Eds.): *Stochastic Dynamics Out of Equilibrium*, PROMS 282, pp. 413–436, 2019.
https://doi.org/10.1007/978-3-030-15096-9_13

nutrients to it. Once blood and oxygen have reached the hypoxic region, secretion of growth factors stops, anti-angiogenic substances may be secreted and a regular vessel network may have been put in place, after pruning capillaries with insufficient blood flow. In normal functioning, angiogenic and anti-angiogenic activities balance. Imbalance may result in many diseases including cancer [6]. In fact, after a tumor installed in tissue reaches some 2 mm size, it needs additional nutrients and oxygen to continue growing. Its hypoxic cells secrete growth factors and induce angiogenesis. Unlike normal cells, cancerous ones continue issuing growth factors and attracting blood vessels, which also supply them with a handy transportation system to reach other organs in the body.

Tumor-induced angiogenesis research started with Folkman's pioneering work in 1971 [6]. In addition to vast experimental research [7], models and theory [8] substantially contribute to understanding angiogenesis and developing therapies. In angiogenesis, events happening in cellular and subcellular scales unchain endothelial cell motion and proliferation and build millimeter scale blood sprouts and networks thereof [2–5]. Models range from very simple to extraordinarily complex and often try to illuminate some particular mechanism; see the review [8]. Realistic microscopic models involve postulating mechanisms and a large number of parameters that cannot be directly estimated from experiments, but they often yield qualitative predictions that can be tested. An important challenge is to extract mesoscopic and macroscopic descriptions of angiogenesis from the diverse microscopic models.

During angiogenesis, the relevant branching, growth and anastomosis (vessel fusion) stochastic processes of the capillary network at the microscale are strongly coupled to the interacting underlying biochemical and mechanical fields at the macroscale. In Sect. 2, we consider a hybrid mesoscale tip cell model that involves stochastic branching, anastomosis and extension of active vessel tip cells with reaction-diffusion growth factor fields [9]. Numerical simulations of the model show that anastomosis prevents indefinite proliferation of active vessel tips [10]. Then fluctuations about the mean of the density of active tips are not small and the stochastic process is not self-averaging. However, as shown in Sect. 3, it is possible to obtain a deterministic description of the density of active tips for ensemble averages over replicas of the stochastic process. The deterministic description consists of an integro-partial differential equation for the density of active vessel tips coupled to a reaction-diffusion equation for the growth factor [9,10]. As shown in Sect. 4, the evolution of active tips from a primary vessel to a hypoxic region adopts the form of an advancing soliton-like wave that can be characterized by ordinary differential equations for its position, velocity and a size parameter [11,12]. These results may pave the way to assess optimal control of angiogenesis and therapies based on it.

What are the implications of our work? As described in Sect. 5, there are other models related to ours in which the vessel extension is described by random walks [13,14], and our methodology may be used to extract deterministic descriptions for the density of active tips amenable to analysis. We could also seek to extend microscopic cellular Potts models (described in Sect. 6) to mesoscales and study

them using our methods. The role of blood flow in remodeling vascular networks is briefly considered in Sect. 7. A quite different approach is presented in Sect. 8. Reaction-diffusion equations for growth factors are coupled to a Cahn-Hilliard type equation for a phase field that is fourth order in space. The phase field has a potential with two minima corresponding to the extracellular matrix and to the advancing blood vessels. There are conditions for the velocity of the capillaries and to create new ones. Further remarks are included in our conclusions in Sect. 9.

2 Langevin Tip Cell Models

Tip cell models assume that the tip cells are motile and non-proliferating whereas stalk cells build the blood vessel following the trajectories of the former. Assuming that the tip cells form point particles, their trajectories constitute the blood vessels advancing toward the hypoxic region. In 1991, Stokes and Lauffenburger considered the capillary sprouts as particles of unit mass subject to chemotactic, friction and white noise forces [15,16]. The distribution of vessel endothelial growth factors (VEGF) issuing from a small circular tumor (or from a small circular hypoxic region) is a known stationary non-uniform function. Associated to each sprout, its cell density satisfies a rate equation that takes into account proliferation, elongation, redistribution of cells from the parent vessel, branching and anastomosis. They did not consider the depletion effect that advancing sprouts would have on the VEGF concentration. Later tip cell models combined a continuum description of fields influencing cell motion (chemotaxis, haptotaxis, ...) with random walk motion of individual sprouts that experience branching and anastomosis. Capasso and Morale [17] used ideas from these approaches to propose a hybrid model of Langevin-Ito stochastic equations for the sprouts undergoing chemotaxis, haptotaxis, branching and anastomosis coupled to reaction-diffusion equations for the continuum fields. In this model, the evolution of the continuum fields is influenced by the growing capillary network through smoothed (or mollified) versions thereof [18]. Capasso and Morale also attempted to derive a continuum equation for the density of moving tip cells from the stochastic equations but could not account for branching and anastomosis [17]. In what follows, we present a simplified hybrid model that ignores haptotaxis and derive a deterministic description for the density of active tips [9,10,19]. As in the Capasso-Morale model, the influence of haptotaxis can be included by adding reaction-diffusion equations for fibronectin and matrix-degrading enzymes [20]. The influence of blood circulation through the newly created blood vessels and secondary branching therefrom can be modeled as in [21].

We shall consider a slab geometry as indicated in Fig. 1, which is the result of a numerical simulation of the stochastic model. The extension of the ith capillary sprout with position $\mathbf{X}^i(t)$ and velocity $\mathbf{v}^i(t)$ is given by the nondimensional Langevin-Ito stochastic equation

$$\begin{aligned} d\mathbf{X}^i(t) &= \mathbf{v}^i(t)\,dt \\ d\mathbf{v}^i(t) &= \beta\left[-\mathbf{v}^i(t) + \mathbf{F}\big(C(t,\mathbf{X}^i(t))\big)\right]dt + \sqrt{\beta}\,d\mathbf{W}^i(t) \end{aligned} \tag{1}$$

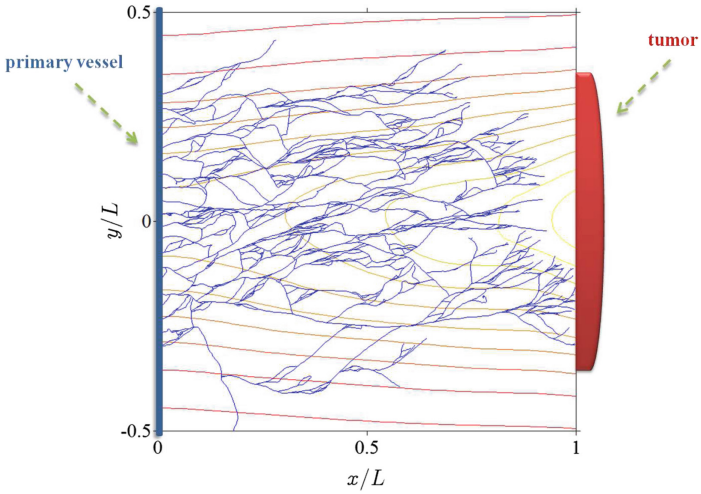

Fig. 1. Network of blood vessels simulated by the stochastic model of tumor induced angiogenesis. The level curves of the density of the tumor angiogenic factor (vessel endothelial growth factor) are also depicted, [11].

for $t > T^i$ (T^i is the random birth time of the ith tip). Here $C(t, \mathbf{x})$ is the VEGF concentration. At time T^i , the velocity of the newly created tip is selected out of a normal distribution with mean $\mathbf{v}_0$ and variance σ_v^2, while the probability that a tip branches from one of the existing ones during an infinitesimal time interval $(t, t + dt]$ is proportional to

$$\sum_{i=1}^{N(t,\omega)} \alpha(C(t, \mathbf{X}^i(t)))dt. \tag{2}$$

Here $N(t, \omega)$ is the number of tips at time t for a realization ω of the stochastic process and

$$\alpha(C) = \frac{A\,C}{C+1}, \tag{3}$$

where A is a positive constant. We ignore secondary angiogenesis from newly formed capillaries [21]. The tip i disappears at a later random time Θ^i, either by reaching the hypoxic region or by anastomosis, i.e., by meeting another capillary. At time t, anastomosis for the ith tip occurs at a point $\mathbf{x}$ such that $\mathbf{X}^i(t) = \mathbf{x}$ and $\mathbf{X}^j(s) = \mathbf{x}$ for another tip that was at $\mathbf{x}$ previously, at time $s < t$. Anastomosis reduces the importance of secondary angiogenesis, because: (i) newly formed capillaries need some time to mature and issue tip cells from their walls, and (ii) secondary branches appear in a crowded environment and their life before they

anastomose is typically short. In (1), $\mathbf{W}^i(t)$ are i.i.d. Brownian motions, and β (friction coefficient) is a positive parameter [9,10,12]. The chemotactic force $\mathbf{F}$ controlling tip cell migration in response to the VEGF released by hypoxic cells is

$$\mathbf{F}(C) = \frac{\delta_1}{1 + \Gamma_1 C} \nabla_x C, \tag{4}$$

where δ_1, and Γ_1 are positive parameters. The VEGF diffuses and is consumed by advancing vessel tips according to [10]

$$\frac{\partial C}{\partial t}(t, \mathbf{x}) = \kappa_c \Delta_x C(t, \mathbf{x}) - \chi_c C(t, \mathbf{x}) \left| \sum_{i=1}^{N(t,\omega)} \mathbf{v}^i(t)\, \delta_{\sigma_x}(\mathbf{x} - \mathbf{X}^i(t)) \right|. \tag{5}$$

Here κ_c and χ_c are positive parameters, while δ_{σ_x} is a regularized delta function (e.g., a Gaussian with standard deviation σ_x). We are assuming that extending the vessel consumes VEGF. As the vessel extends a length $|\mathbf{v}^i(t)|\, dt$ during the time interval between t and $t + dt$, the consumption should be proportional to $|\mathbf{v}^i(t)|$. The resulting equation for the VEGF is then

$$\frac{\partial C}{\partial t}(t, \mathbf{x}) = \kappa_c \Delta_x C(t, \mathbf{x}) - \tilde{\chi}_c C(t, \mathbf{x}) \sum_{i=1}^{N(t,\omega)} |\mathbf{v}^i(t)|\, \delta_{\sigma_x}(\mathbf{x} - \mathbf{X}^i(t)). \tag{6}$$

The difference between the more appropriate model equation (6) and (5) could be considerable for situations where tip cells are moving in all directions. However, for the parameters and the slab geometry considered in the numerical simulations presented in this paper, this difference is negligible (it amounts to having $\tilde{\chi}_c = 1.28\chi_c$ in the previous equation). Initial and boundary conditions for the VEGF field C have been proposed in [9,10].

The concentration of all vessels per unit volume in the physical space, at time t (i.e., the vessel network $\mathbf{X}(t, \omega)$) is [10]

$$\delta(\mathbf{x} - \mathbf{X}(t, \omega)) = \int_0^t \sum_{i=1}^{N(s,\omega)} \delta_{\sigma_x}(\mathbf{x} - \mathbf{X}^i(s, \omega))\, ds. \tag{7}$$

3 Deterministic Description

We shall see that we can understand the results of numerical simulations of the stochastic process described in the previous section by first finding a deterministic description of the density of active tips. The latter evolves in the form of a slowly varying soliton-like wave that we can analyze. Without performing numerical simulations of the stochastic process, we could guess that such a

deterministic description could hold whenever the number of active tips arising from branching becomes very large. In such a case, we could use the law of large numbers to achieve such a description. This was the point of view adopted in the papers [9,17]. However, anastomosis kills off so many active vessel tips that their number hardly grows to a hundred. Then we need a different point of view in order to derive a deterministic description. The alternative is the Gibbsian idea of considering an ensemble of replicas of the original stochastic process and carrying out arithmetic averages over the number of replicas.

We can find a deterministic description of the stochastic model for the densities of active vessel tips and the vessel tip flux, defined as ensemble averages over a sufficient number $\mathscr{N}$ of replicas (realizations) ω of the stochastic process:

$$p_{\mathscr{N}}(t,\mathbf{x},\mathbf{v}) = \frac{1}{\mathscr{N}} \sum_{\omega=1}^{\mathscr{N}} \sum_{i=1}^{N(t,\omega)} \delta_{\sigma_x}(\mathbf{x}-\mathbf{X}^i(t,\omega))\, \delta_{\sigma_v}(\mathbf{v}-\mathbf{v}^i(t,\omega)), \tag{8}$$

$$\tilde{p}_{\mathscr{N}}(t,\mathbf{x}) = \frac{1}{\mathscr{N}} \sum_{\omega=1}^{\mathscr{N}} \sum_{i=1}^{N(t,\omega)} \delta_{\sigma_x}(\mathbf{x}-\mathbf{X}^i(t,\omega)), \tag{9}$$

$$\mathbf{j}_{\mathscr{N}}(t,\mathbf{x}) = \frac{1}{\mathscr{N}} \sum_{\omega=1}^{\mathscr{N}} \sum_{i=1}^{N(t,\omega)} \mathbf{v}^i(t,\omega)\delta_{\sigma_x}(\mathbf{x}-\mathbf{X}^i(t,\omega)). \tag{10}$$

As $\mathscr{N} \to \infty$, these ensemble averages tend to the tip density $p(t,\mathbf{x},\mathbf{v})$, the marginal tip density $\tilde{p}(t,\mathbf{x})$, and the tip flux $\mathbf{j}(t,\mathbf{x})$, respectively.

Figures 2 and 3 show the outcomes of typical simulations of ensemble averaged marginal densities: The two-dimensional lump shown in Fig. 2 is created at the primary vessel at $x = 0$ and marches to the hypoxic region at $x = 1$. Its profile along the x axis is the soliton-like wave shown in Fig. 3.

Reference [10] shows that the angiogenesis model has a deterministic description based on the following equation for the density of vessel tips, $p(t,\mathbf{x},\mathbf{v})$,

$$\frac{\partial p}{\partial t}(t,\mathbf{x},\mathbf{v}) = \alpha(C(t,\mathbf{x}))\, p(t,\mathbf{x},\mathbf{v})\delta_{\sigma_v}(\mathbf{v}-\mathbf{v}_0) - \Gamma\, p(t,\mathbf{x},\mathbf{v}) \int_0^t \tilde{p}(s,\mathbf{x})\, ds$$
$$-\mathbf{v}\cdot\nabla_x p(t,\mathbf{x},\mathbf{v}) - \beta\nabla_v\cdot[(\mathbf{F}(C(t,\mathbf{x})) - \mathbf{v})p(t,\mathbf{x},\mathbf{v})] + \frac{\beta}{2}\Delta_v p(t,\mathbf{x},\mathbf{v}), \tag{11}$$

$$\tilde{p}(t,\mathbf{x}) = \int p(t,\mathbf{x},\mathbf{v}')\, d\mathbf{v}'. \tag{12}$$

The two first terms on the right hand side of (11) correspond to vessel tip branching – from Eqs. (2) and (3) – and anastomosis, respectively. While the branching term follows from (2) and (3) in a straightforward manner, deducing the anastomosis integral term is the real breakthrough from past work achieved in [9]. The anastomosis coefficient, Γ, has to be fitted by comparison of the numerical solution of the deterministic equations and ensemble averages of the stochastic description, [10]. The other terms on the right hand side of (11) are in the Fokker-Planck equation that corresponds to the Langevin equation (1) in the usual manner [22]. While the branching term follows directly from the

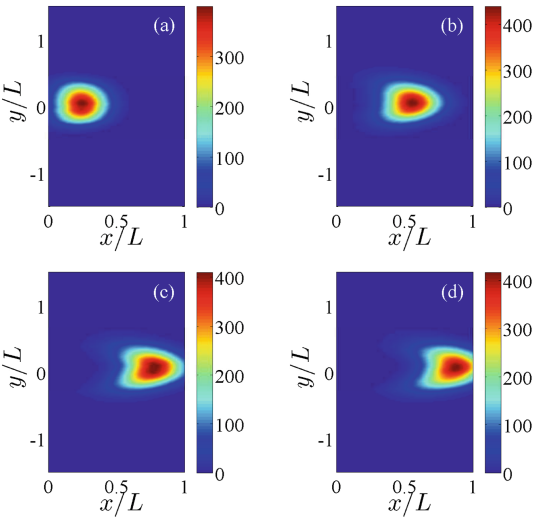

Fig. 2. Marginal density of active vessel tips resulting from an average over 400 replicas of the stochastic process according to Eq. (9) at four different times: (a) 12 h, (b) 24 h, (c) 32 h, and (d) 36 h. At these times, the numbers of active tips are (a) 56, (b) 69, (c) 72, and (d) 66, [10].

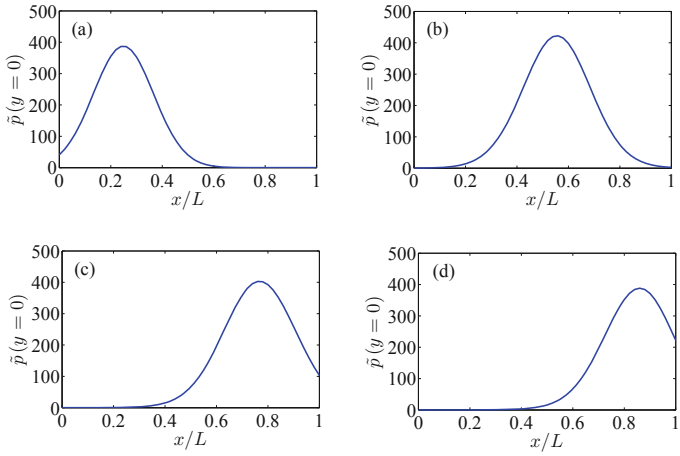

Fig. 3. Marginal density of active vessel tips at the x axis resulting from an average over 400 replicas of the stochastic process as in Fig. 2. The primary vessel at $x = 0$ issues a pulse that marches toward the hypoxic region at $x = 1$, [10].

stochastic branching process, anastomosis occurs when a moving vessel tip at time $t > 0$ encounters a preexisting vessel whose tip was at the same place at an earlier time $s < t$. At time t, a moving vessel tip can reach an area $d\mathbf{x}$ about $\mathbf{x}$ that is either unoccupied or occupied by another vessel. In the latter case, it anastomoses. The occupation time density of the area $d\mathbf{x}$ about $\mathbf{x}$ is proportional to $\int_0^t \tilde{p}(s,\mathbf{x})\,ds$ - the ensemble average of the vessel network density (7). Then the rate of anastomosis should be proportional to $p(t,\mathbf{x},\mathbf{v})$ times this occupation time density [10]. Equation (5) becomes

$$\frac{\partial C}{\partial t}(t,\mathbf{x}) = \kappa_c \Delta_x C(t,\mathbf{x}) - \chi_c C(t,\mathbf{x})\,|\mathbf{j}(t,\mathbf{x})|, \tag{13}$$

where $\mathbf{j}(t,\mathbf{x})$ is the current density (flux) vector at any point $\mathbf{x}$ and any time $t \geq 0$,

$$\mathbf{j}(t,\mathbf{x}) = \int \mathbf{v}' p(t,\mathbf{x},\mathbf{v}')\,d\mathbf{v}'. \tag{14}$$

Equation (6) becomes (13) in which $\int |\mathbf{v}'|\,p(t,\mathbf{x},\mathbf{v}')\,d\mathbf{v}'$ replaces $|\mathbf{j}(t,\mathbf{x})|$.

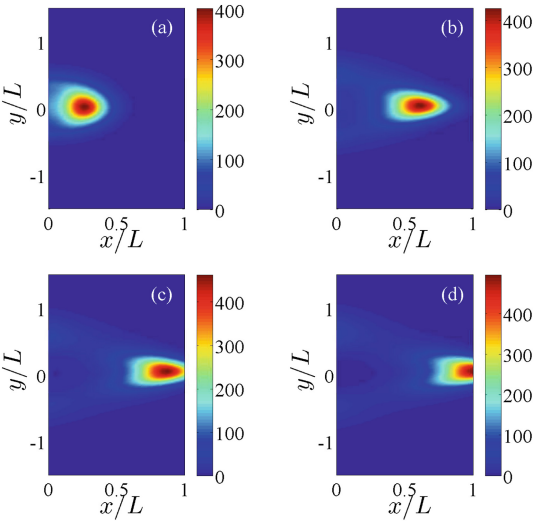

Fig. 4. Marginal density of active vessel tips resulting from a numerical simulation of the deterministic equations with appropriate boundary conditions for the same times as in Fig. 2 [9,10]. Better agreement between both descriptions requires fine tuning of the boundary conditions.

Figure 4 shows that the outcome of a numerical simulation of the deterministic description is similar to that of the stochastic process.

Carpio and collaborators have shown that the deterministic system of Eqs. (11)–(13) together with appropriate boundary and initial conditions has a unique solution that depends smoothly on parameters [23,24]. The proof that the deterministic description (11) follows from ensemble averages of the stochastic process

as described here is an important *open problem*. Anastomosis is a random event that depends on the past history of each realization of the stochastic process. Killing process with memory of this type have been studied formally before. However, the densities (8)–(10) are ensemble averages over infinitely many different realizations, which are, by definition, independent from each other. This could be important in a mathematical investigation of these processes.

In a recent paper [25], Capasso and Flandoli have proved an important convergence result for the deterministic description. They consider an appropriately modified stochastic process for d-dimensional angiogenesis on the whole space that also includes secondary branching at random points of existing capillaries. In the limit as the initial number of tips N_0 tends to infinity, they prove that a relative tip density (scaled with the initial number of tips) converges in probability. The limiting relative tip density satisfies in a weak sense a deterministic integro partial differential equation. In this equation, integrals over time also appear at the source term due to secondary angiogenesis. As explained before, the memory source term due to secondary angiogenesis is likely to be small compared to the local source term considered in (11). Capasso and Flandoli also prove that the number of tips at any given time $t \in [0, T]$ is bounded by a factor $e^{\lambda T} N_0$, with $\lambda > 0$. It would be interesting to see whether the limit as $N_0 \to \infty$ can be replaced by ensemble averages at least in the 2D case. Similarly, comparison of numerical solutions of the deterministic description on an appropriate geometry and averages of the stochastic process would help understanding the implications of the rigorous results in [25].

4 Soliton and Collective Coordinates

In the overdamped limit of negligible inertia in (1), we obtain the simpler Langevin-Ito equation: $d\mathbf{X}^i(t) \approx \mathbf{F}(C(t, \mathbf{X}^i(t)))\, dt + \beta^{-1/2} d\mathbf{W}^i(t)$ [11]. By using the Chapman-Enskog perturbation method whose details are explained in [12], it is then possible to derive the following reduced equation for the marginal tip density,

$$\frac{\partial \tilde{p}}{\partial t} + \nabla_x \cdot (\mathbf{F}\tilde{p}) - \frac{1}{2\beta} \Delta_x \tilde{p} = \mu\, \tilde{p} - \Gamma \tilde{p} \int_0^t \tilde{p}(s, \mathbf{x})\, ds, \tag{15}$$

$$\mu = \frac{\alpha}{\pi} \left[1 + \frac{\alpha}{2\pi\beta(1 + \sigma_v^2)} \ln\left(1 + \frac{1}{\sigma_v^2} \right) \right]. \tag{16}$$

The drift terms in Eq. (15) are those corresponding to the simpler Langevin-Ito equation for $\mathbf{X}^i(t)$ that results in the overdamped limit. The birth and death terms are obtained by integration of the corresponding ones on right hand side of (11) over velocity. However, the perturbation procedure changes the coefficient $\alpha(C)$ to the related function $\mu(C)$ in (16) [12]. Equation (15) has the following soliton-like solution for constant $\mathbf{F} = (F_x, F_y)$, μ, and zero diffusion, $1/\beta = 0$:

$$\tilde{p}_s = \frac{(2K\Gamma + \mu^2)c}{2\Gamma(c - F_x)} \operatorname{sech}^2 \left[\frac{\sqrt{2K\Gamma + \mu^2}}{2(c - F_x)} (x - X(t)) \right], \quad \dot{X} \equiv \frac{dX}{dt} = c, \tag{17}$$

where K is a constant. In fact [11], consider $\tilde{p}_s = \partial P(x-ct)/\partial t = -c\,P'(\xi)$, $\xi = x - ct$, which, inserted in (15) with $1/\beta = 0$, yields

$$(F_x - c)P'' = \mu P' - \Gamma P P' \Longrightarrow (c - F_x)P' = \frac{\Gamma}{2}P^2 - K - \mu P.$$

Setting $P = \nu\tanh(\lambda\xi)+\mu/\Gamma$, we find $\nu^2 = (\mu^2+2K\Gamma)/\Gamma^2$ and $2\nu\lambda(c-F_x)/\Gamma = -\nu^2$, thereby obtaining

$$P = \frac{\mu}{\Gamma} - \frac{\sqrt{2K\Gamma+\mu^2}}{\Gamma}\tanh\left[\frac{\sqrt{2K\Gamma+\mu^2}}{2(c-F_x)}(\xi-\xi_0)\right].$$

Here ξ_0 is a constant of integration. Thus $\tilde{p}_s = \partial P/\partial t = -cP'$ is given by (17).

Note that the source terms (branching and anastomosis) in Eqs. (11) and (16) are crucial for the soliton solution (17) to exist. Their absence in all developments previous to [9] explains that they could not go beyond numerical simulations of the stochastic process.

Numerical simulations on a slab geometry show that the marginal tip density evolves toward (17) after an initial stage [11,12]. *It is an open problem to prove this stability result even for a one-dimensional version of Eq. (15) on the whole real line and having constant values of* $\mathbf{F}$ *and* μ.

A small diffusion and slowly varying continuum field C produce a moving soliton whose shape and speed are slowly changing. We can find them by deducing evolution equations for the *collective coordinates* K, c, and X [11,12]. Then the marginal density profile at $y = 0$ can be reconstructed from (17) with spatially averaged F_x and μ [12]. Note that $\tilde{p}_s$ is a function of $\xi = x - X$ and also of $\mathbf{x}$ and t through $C(t,\mathbf{x})$,

$$\tilde{p}_s = \tilde{p}_s\left(\xi; K, c, \mu(C), F_x\left(C, \frac{\partial C}{\partial x}\right)\right). \tag{18}$$

We assume that the time and space variations of C, which appear when $\tilde{p}_s$ is differentiated with respect to t or x, produce terms that are small compared to $\partial\tilde{p}_s/\partial\xi$. As explained in [12], we shall consider that $\mu(C)$ is approximately constant, ignore $\partial C/\partial t$ because the VEGF concentration varies slowly (the dimensionless coefficients κ_c and χ_c appearing in the VEGF equation (13) are very small according to Table 2 of [12]) and ignore $\partial^2\tilde{p}_s/\partial i\partial j$, where $i, j = K$, F_x. We now insert (17) into (15), thereby obtaining

$$\left(F_x - \dot{X}\right)\frac{\partial\tilde{p}_s}{\partial\xi} + \frac{\partial\tilde{p}_s}{\partial K}\dot{K} + \frac{\partial\tilde{p}_s}{\partial c}\dot{c} - \frac{1}{2\beta}\left(\frac{\partial^2\tilde{p}_s}{\partial\xi^2} + 2\frac{\partial^2\tilde{p}_s}{\partial\xi\partial F_x}\frac{\partial F_x}{\partial x} + \frac{\partial\tilde{p}_s}{\partial F_x}\Delta_x F_x\right)$$
$$+\tilde{p}_s\nabla_x\cdot\mathbf{F} + \frac{\partial\tilde{p}_s}{\partial F_x}\left(\frac{\partial F_x}{\partial t} + \mathbf{F}\cdot\nabla_x F_x\right) = \mu\tilde{p}_s - \Gamma\tilde{p}_s\int_0^t \tilde{p}_s dt. \tag{19}$$

Equation (15) with $1/\beta = 0$ and constant $\mathbf{F}$ and μ has the soliton solution (17). Using this fact, we can eliminate the first term on the left hand side of (19) and

also the right hand side thereof. Equation (19) then becomes

$$\frac{\partial \tilde{p}_s}{\partial K}\dot{K} + \frac{\partial \tilde{p}_s}{\partial c}\dot{c} = \mathscr{A}, \tag{20}$$

$$\mathscr{A} = \frac{1}{2\beta}\frac{\partial^2 \tilde{p}_s}{\partial \xi^2} - \tilde{p}_s \nabla_x \cdot \mathbf{F} - \frac{\partial \tilde{p}_s}{\partial F_x}\left(\mathbf{F}\cdot\nabla_x F_x - \frac{1}{2\beta}\Delta_x F_x\right) + \frac{1}{\beta}\frac{\partial^2 \tilde{p}_s}{\partial \xi \partial F_x}\frac{\partial F_x}{\partial x}. \tag{21}$$

We now find collective coordinate equations (CCEs) for K and c. As the lump-like angiton moves on the x axis, we set $y = 0$ to capture the location of its maximum. On the x axis, the profile of the angiton is the soliton (17). We first multiply (20) by $\partial \tilde{p}_s/\partial K$ and integrate over x. We consider a fully formed soliton far from primary vessel and hypoxic region. As it decays exponentially for $|\xi| \gg 1$, the soliton is considered to be localized on some finite interval $(-\mathscr{L}/2, \mathscr{L}/2)$. The coefficients in the soliton formula (17) and the coefficients in (21) depend on the VEGF concentration at $y = 0$, therefore they are functions of x and time and get integrated over x. The VEGF concentration varies slowly on the support of the soliton, and therefore we can approximate the integrals over x by [12]

$$\int_{\mathscr{I}} F(\tilde{p}_s(\xi; x, t), x)dx \approx \frac{1}{\mathscr{L}}\int_{\mathscr{I}}\left(\int_{-\mathscr{L}/2}^{\mathscr{L}/2} F(\tilde{p}_s(\xi; x, t), x)d\xi\right)dx. \tag{22}$$

The interval $\mathscr{I}$ over which we integrate should be large enough to contain most of the soliton, of extension $\mathscr{L}$. Thus the CCEs hold only after the initial soliton formation stage. Near the primary vessel and near the hypoxic region, the boundary conditions affect the soliton and we should exclude intervals near them from $\mathscr{I}$. We shall specify the integration interval $\mathscr{I}$ below. Acting similarly, we multiply (20) by $\partial \tilde{p}_s/\partial c$ and integrate over x. From the two resulting formulas, we then find $\dot{K}$ and $\dot{c}$ as fractions. The factors $1/\mathscr{L}$ cancel out from their numerators and denominators. As the soliton tails decay exponentially to zero, we can set $\mathscr{L} \to \infty$ and obtain the following CCEs [12]

$$\dot{K} = \frac{\int_{-\infty}^{\infty}\frac{\partial \tilde{p}_s}{\partial K}\mathscr{A}d\xi \int_{-\infty}^{\infty}\left(\frac{\partial \tilde{p}_s}{\partial c}\right)^2 d\xi - \int_{-\infty}^{\infty}\frac{\partial \tilde{p}_s}{\partial c}\mathscr{A}d\xi \int_{-\infty}^{\infty}\frac{\partial \tilde{p}_s}{\partial K}\frac{\partial \tilde{p}_s}{\partial c}d\xi}{\int_{-\infty}^{\infty}\left(\frac{\partial \tilde{p}_s}{\partial K}\right)^2 d\xi \int_{-\infty}^{\infty}\left(\frac{\partial \tilde{p}_s}{\partial c}\right)^2 d\xi - \left(\int_{-\infty}^{\infty}\frac{\partial \tilde{p}_s}{\partial c}\frac{\partial \tilde{p}_s}{\partial K}d\xi\right)^2}, \tag{23}$$

$$\dot{c} = \frac{\int_{-\infty}^{\infty}\frac{\partial \tilde{p}_s}{\partial c}\mathscr{A}d\xi \int_{-\infty}^{\infty}\left(\frac{\partial \tilde{p}_s}{\partial K}\right)^2 d\xi - \int_{-\infty}^{\infty}\frac{\partial \tilde{p}_s}{\partial K}\mathscr{A}d\xi \int_{-\infty}^{\infty}\frac{\partial \tilde{p}_s}{\partial K}\frac{\partial \tilde{p}_s}{\partial c}d\xi}{\int_{-\infty}^{\infty}\left(\frac{\partial \tilde{p}_s}{\partial K}\right)^2 d\xi \int_{-\infty}^{\infty}\left(\frac{\partial \tilde{p}_s}{\partial c}\right)^2 d\xi - \left(\int_{-\infty}^{\infty}\frac{\partial \tilde{p}_s}{\partial c}\frac{\partial \tilde{p}_s}{\partial K}d\xi\right)^2}. \tag{24}$$

In these equations, all terms varying slowly in space have been averaged over the interval $\mathscr{I}$. The last term in (21) is odd in ξ and does not contribute to the integrals in (23) and (24) whereas all other terms in (21) are even in ξ and do contribute. The integrals appearing in (23) and (24) are calculated in [12]. The resulting CCEs are

$$\dot{K} = \frac{(2K\Gamma+\overline{\mu}^2)^2}{4\Gamma\beta(c-\overline{F_x})^2}\,\frac{\frac{4\pi^2}{75}+\frac{1}{5}+\left(\frac{2\overline{F_x}}{5c}-\frac{2\pi^2}{75}-\frac{9}{10}\right)\frac{\overline{F_x}}{c}}{\left(1-\frac{4\pi^2}{15}\right)\left(1-\frac{\overline{F_x}}{2c}\right)^2}$$
$$-\frac{2K\Gamma+\overline{\mu}^2}{\Gamma c\left(2-\frac{\overline{F_x}}{c}\right)}\left(c\overline{\nabla_x\cdot\mathbf{F}}+\overline{\mathbf{F}\cdot\nabla_x F_x}-\frac{\overline{\Delta_x F_x}}{2\beta}\right), \tag{25}$$

$$\dot{c} = -\frac{7(2K\Gamma+\overline{\mu}^2)}{20\beta(c-\overline{F_x})}\,\frac{1-\frac{4\pi^2}{105}}{\left(1-\frac{4\pi^2}{15}\right)\left(1-\frac{\overline{F_x}}{2c}\right)}+\frac{\overline{\mathbf{F}\cdot\nabla_x F_x}-(c-\overline{F_x})\overline{\nabla_x\cdot\mathbf{F}}-\frac{\overline{\Delta_x F_x}}{2\beta}}{2-\frac{\overline{F_x}}{c}}, \tag{26}$$

$$\overline{g(x,y)} = \frac{1}{\mathscr{I}}\int_{\mathscr{I}} g(x,0)\,dx, \tag{27}$$

in which the functions of $C(t,x,y)$ have been averaged over the interval $\mathscr{I}$ after setting $y=0$. We expect the CCEs (25)–(26) to describe the mean behavior of the soliton whenever it is far from primary vessel and hypoxic region.

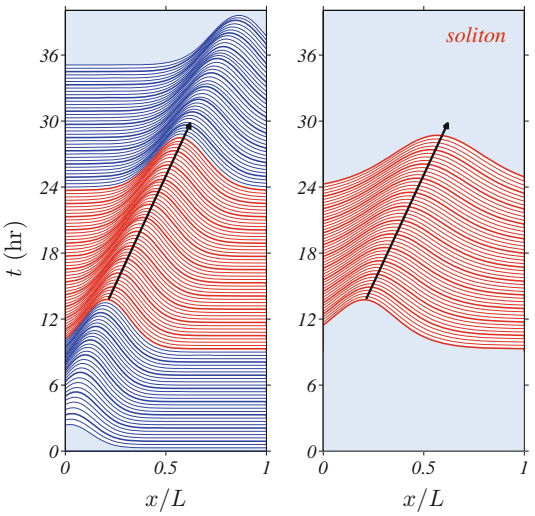

Fig. 5. Comparison of the marginal tip density profile $\tilde{p}(t,x,0)$ (obtained from the stochastic description averaged over 400 replicas) to that of the moving soliton, [11].

Both deterministic or stochastic simulations show that the soliton is formed after some time $t_0 = 0.2$ (10 h) following angiogenesis initiation. To find the soliton evolution afterwards, we need to solve the CCEs (25)–(26), in which the spatial averages depend on an interval $x \in \mathscr{I}$, which should exclude regions affected by boundaries. We calculate the spatially averaged coefficients in (25)–(26) by: (i) approximating all differentials by second order finite differences, (ii) setting $y = 0$, and (iii) averaging the coefficients from $x = 0$ to 0.6 by taking the arithmetic mean of their values at all grid points in the interval

$\mathscr{I} = (0, 0.6]$. For $x > 0.6$, the boundary condition at $x = 1$ influences the outcome and therefore we leave values for $x > 0.6$ out of the averaging [12]. The initial conditions for the CCEs are set as follows. $X(t_0) = X_0$ is the location of the marginal tip density maximum, $\tilde{p}(t_0, x = X_0, 0)$. We find $X_0 = 0.2$ from the stochastic description. We set $c(t_0) = c_0 = X_0/t_0$. $K(t_0) = K_0$ is determined so that the maximum marginal tip density at $t = t_0$ coincides with the soliton peak. This yields $K_0 = 39$. Solving the CCEs (25)–(26) with these initial conditions and using (17), we obtain the curves depicted in Fig. 5.

5 Random Walk Tip Cell Models

These models describe the extension of blood vessels by random walks biased by chemotaxis or haptotaxis instead of using Langevin equations. The first such model, due to Anderson and Chaplain [13], is based on a reaction-diffusion description of angiogenesis. They consider a continuity equation for the density of endothelial cells (ECs) n (with zero-flux boundary conditions) coupled to equations for the VEGF and fibronectin densities, C and f, respectively. In nondimensional form, these equations are [13]:

$$\frac{\partial n}{\partial t} = D\Delta n - \nabla\cdot\left(\frac{\chi}{1+\alpha C} n\nabla C\right) - \nabla\cdot(\rho n\nabla f), \tag{28}$$

$$\frac{\partial f}{\partial t} = \beta n - \gamma n f, \tag{29}$$

$$\frac{\partial C}{\partial t} = -\eta n C. \tag{30}$$

Here all parameters are positive. The three terms on the right hand side of (28) correspond to diffusion of ECs, chemotaxis and haptotaxis, respectively. Note that chemotaxis has the same form in this equation as in (11) with p replaced by n. Haptotaxis follows the gradient of fibronectin in the extracellular matrix. Note that proliferation and death of ECs are not contemplated by (28). In the next step, these equations are solved by an explicit Euler method in time and finite differences. The resulting equation for $n(t, x, y) \approx n^q_{l,m}$,

$$n^{q+1}_{l,m} = n^q_{l,m} W_0 + n^q_{l+1,m} W_1 + n^q_{l-1,m} W_2 + n^q_{l,m+1} W_3 + n^q_{l,m-1} W_4, \tag{31}$$

has the same form as a master equation for a random walk [22], except that the "transition probabilities" W_0 (staying), W_1 (moving to the left), W_2 (moving to the right), W_3 (moving downwards), and W_4 (moving upwards) are not normalized. However, this is easily fixed by defining

$$\mathscr{W}_i = \frac{W_i}{\sum_{j=0}^{4} W_j}, \quad i = 0, 1, \ldots, 4, \tag{32}$$

as new transition probabilities. The random walk associated to these transition probabilities represents extension of vessel tips and replaces the Langevin equation (1). Branching and anastomosis are introduced as in the Langevin tip cell

model, except that the tips have to wait some *maturity* time after branching before they are allowed to branch again. It should be straightforward to find equations for the density of active vessel tips by using the theory described in previous sections.

The Anderson-Chaplain idea is easy to implement starting from continuum models of angiogenesis (and therefore it can be immediately generalized by including more taxis mechanisms, influence of antiangiogenic factors [26], etc.), but it has the drawback of having to rely on the finite difference grid or lattice. Another drawback is that the transition probabilities extracted from a finite difference code may not always be non-negative. A few years later, Plank and Sleeman fixed both these drawbacks. They proposed non-lattice models independent of the grid [14] using biased circular random walk models previously introduced by Hill and Häder for swimming microorganisms [27]. If $\theta(t)$ is a continuous random walk on the unit circle biased by chemo and haptotaxis [14], the trajectory of the corresponding tip cell is

$$\frac{d\mathbf{x}}{dt} = v_0\,(\cos\theta(t), \sin\theta(t)). \tag{33}$$

Thus the tip cells have the same speed v_0, directions given by $\theta(t)$ and their trajectories do not have to follow points on a lattice. While branching and anastomosis are modeled as in Sect. 2, the extensions of vessel tips are described by (33) and the biased circular random walk instead of Langevin equations. The master equation for the circular random walk is [14]

$$\frac{dP_n}{dt} = \hat{\tau}^+_{n-1}P_{n-1} + \hat{\tau}^-_{n+1}P_{n+1} - (\hat{\tau}^+_n + \hat{\tau}^-_n)P_n, \tag{34}$$

$$\hat{\tau}^\pm_n = 2\lambda\frac{\tau\left(n\delta \pm \frac{\delta}{2}\right)}{\tau\left(n\delta + \frac{\delta}{2}\right) + \tau\left(n\delta - \frac{\delta}{2}\right)}. \tag{35}$$

As $\delta \to 0$ and $n \to \infty$ so that $n\delta = \theta$, the master equation (34) becomes the Fokker-Planck equation [14]

$$\frac{\partial P}{\partial t}(t,\theta) = D\frac{\partial}{\partial\theta}\left[P(t,\theta)\frac{\partial}{\partial\theta}\left(\ln\frac{P(t,\theta)}{\tau(\theta)}\right)\right], \tag{36}$$

with $D = \lambda\delta^2$ for $P(t,\theta) = P(t,n\delta) = P_n(t)$. Chemo and haptotaxis are included in the model through the transition probability

$$\tau(\theta) = \frac{\exp[d_C\cos(\theta-\theta_C) + d_f\cos(\theta-\theta_f)]}{\int_{-\pi}^{\pi}\exp[d_C\cos(s-\theta_C) + d_f\cos(s-\theta_f)]\,ds}, \tag{37}$$

$$\tan\theta_C = \frac{\nabla C}{|\nabla C|}, \quad \tan\theta_f = \frac{\nabla f}{|\nabla f|}. \tag{38}$$

Here $\tau(\theta)$ is the stationary probability density of the Fokker-Planck equation (36).

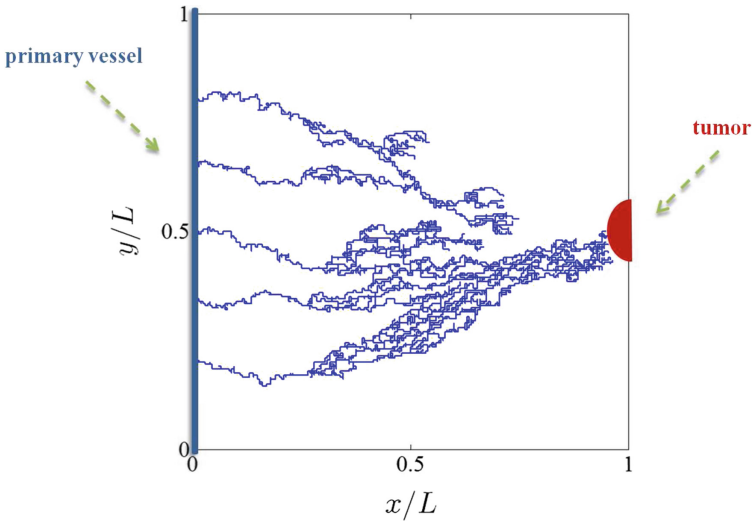

Fig. 6. Sketch of the geometry for angiogenesis from a primary blood vessel to a circular tumor calculated by using the Anderson-Chaplain model.

An extension of these ideas to 2D random walks produces a system with non-negative transition probabilities [14]. Instead of (34), we may write the 2D master equation

$$\frac{dP_{n,m}}{dt} = \hat{\tau}^{H+}_{n-1,m}P_{n-1,m} + \hat{\tau}^{H-}_{n+1,m}P_{n+1,m} + \hat{\tau}^{V+}_{n,m-1}P_{n,m-1} + \hat{\tau}^{V-}_{n,m+1}P_{n,m+1}$$
$$-(\hat{\tau}^{H+}_{n,m} + \hat{\tau}^{H-}_{n,m} + \hat{\tau}^{V+}_{n,m} + \hat{\tau}^{V-}_{n,m})P_{n,m}, \tag{39}$$

$$\hat{\tau}^{H\pm}_{n,m} = 4\lambda \frac{\tau(w_{n\pm\frac{1}{2},m})}{\tau(w_{n+\frac{1}{2},m}) + \tau(w_{n-\frac{1}{2},m}) + \tau(w_{n,m+\frac{1}{2}}) + \tau(w_{n,m-\frac{1}{2}})}, \tag{40}$$

$$\hat{\tau}^{V\pm}_{n,m} = 4\lambda \frac{\tau(w_{n,m\pm\frac{1}{2}})}{\tau(w_{n+\frac{1}{2},m}) + \tau(w_{n-\frac{1}{2},m}) + \tau(w_{n,m+\frac{1}{2}}) + \tau(w_{n,m-\frac{1}{2}})}. \tag{41}$$

Here $w = (C, f)$ and $\tau(w) = \tau_1(C)\tau_2(f)$, with

$$\tau_1(C) = (1 + \alpha C)^{\frac{\chi}{\alpha D}}, \quad \tau_2(f) = e^{\rho f/D}. \tag{42}$$

Clearly, these transition probabilities are positive and it can be proved that the master equation (39) has (28) as a continuum limit [14]. Active tips, branching and anastomosis are treated as in the Anderson-Chaplain paper [13]. Comparisons between numerical simulations of the Anderson-Chaplain and Plank-Sleeman models are carried out in [14]. Figure 6 shows one realization of the Anderson-Chaplain stochastic process that includes vessel extension, branching and anastomosis.

The random walk models of this Section get their input from continuum equations for ECs, VEGF and fibronectin densities, but the moving vessel tips characterized by the random walks do not affect the continuum fields. Their outcomes are numerical simulations of the stochastic processes, without further elaboration. In contrast to this somewhat artificial setting, the Langevin tip cell model of Sect. 2 is a hybrid model in which active vessel tips and continuum fields are fully coupled. Furthermore, we can derive an equivalent deterministic description from the Langevin tip cell model and analyze it in terms of a soliton-like attractor. This latter elaboration has also been carried out for a Langevin tip cell model that includes chemotaxis and haptotaxis [20]. Now, the master equation becomes a Fokker-Planck equation (corresponding to a Langevin-Ito equation) in the continuum limit [22]. Then we may expect that the master equation with two added source terms similar to those in Eq. (11) describes the stochastic process comprising random walk, branching and anastomosis. This seems to be the case [28].

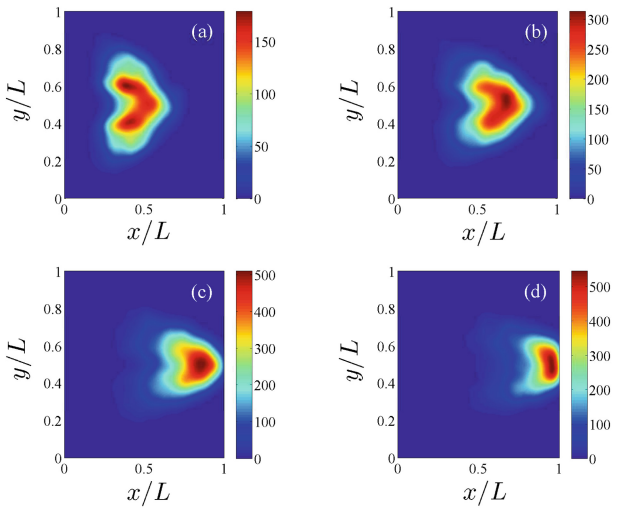

Fig. 7. Density of active vessel tips resulting from an average over 800 replicas of the stochastic process corresponding to reinforced random walk, branching and anastomosis with transition probabilities (40)–(41) at four different times: (a) 5 days, (b) 6 days, (c) 7 days, and (d) 8 days.

When we add source terms to the master equation (39), it becomes the following equation for the density of active vessel tips $\rho_{n,m}(t)$:

$$\frac{d\rho_{n,m}}{dt} = \hat{\tau}^{H+}_{n-1,m}\rho_{n-1,m} + \hat{\tau}^{H-}_{n+1,m}\rho_{n+1,m} + \hat{\tau}^{V+}_{n,m-1}\rho_{n,m-1} + \hat{\tau}^{V-}_{n,m+1}\rho_{n,m+1}$$
$$-(\hat{\tau}^{H+}_{n,m} + \hat{\tau}^{H-}_{n,m} + \hat{\tau}^{V+}_{n,m} + \hat{\tau}^{V-}_{n,m})\rho_{n,m} + \alpha_{n,m}\,\rho_{n,m} - \Gamma_{n,m}\,\rho_{n,m}\int_0^t \rho_{n,m}\,dt. \qquad (43)$$

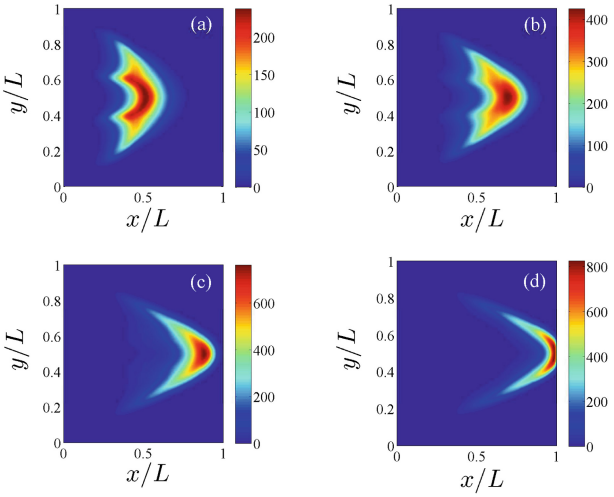

Fig. 8. Density of active vessel tips calculated from the master equation (43) at times: (a) 5 days, (b) 6 days, (c) 7 days, and (d) 8 days.

Figure 7 depicts the active vessel density (9) calculated from ensemble average over replicas of the stochastic process (reinforced random walk, branching and anastomosis) at four different times after angiogenesis starts. Figure 8 shows the solution of the master equation (43) at the same times as in Fig. 7. Both stochastic and deterministic descriptions produce similar results. In particular, the velocity of the patch where most active tips are concentrated is about the same in both descriptions. See [28] for details.

As in the case of the stochastic process including Langevin-Ito equations for vessel extension of Sect. 2, it is an important *open problem* to deduce the master equation (43) from a reinforced random walk process with added branching and anastomosis.

6 Cellular Potts Models

In all the previous models, the cells are treated as point particles. For a more precise view of haptotaxis, i.e., the motion of ECs over the extracellular matrix (ECM), we need to consider adhesion and deformation of the cells. This requires a more microscopic view than that offered by tip cell models or by more complicated models that distinguish between tip and stalk ECs and add extra dynamics for them [8].

Often times, ECs and ECM are modeled by a cellular Potts model (CPM) with Monte Carlo dynamics coupled to continuum fields (elastic fields, VEGF, ...) [29]. Space in these models consists of a lattice whose cells (lattice sites) may be in finitely many different states, denoted by type τ and representing ECs, matrix fibers, tissue cells and interstitial fluid. To account for individual entities

(ECs, fibers, etc), each entity is further associated with a unique identifying number, denoted by σ, that is assigned to every lattice site occupied by it. At every Monte Carlo time step, the cell surface (represented by connected lattice vertices) is updated according to a set of cell behavior rules (e.g., target cell shape and size) that are translated in an energy change. Typically, we select randomly a cell $\mathbf{x}$, assign its type, $\tau(\mathbf{x})$, to a randomly chosen neighbor $\mathbf{x}'$, and update accordingly the total energy of the system, H. Using the Metropolis algorithm, a given update is accepted with probability one if the change in the total energy of the system, ΔH, is reduced and it is accepted with probability $e^{-\beta\Delta H}$ otherwise ($1/\beta$ is the Monte Carlo temperature). The energy in [29] is

$$H = \sum_{\text{sites}} J_{\tau,\tau'}(1-\delta_{\sigma\sigma'}) + \sum_{\text{cells}} \gamma_\tau (a_\sigma - A_\sigma)^2 - \sum_{\text{cells}} \sum_{\text{sites}} \mu_\sigma C(t,\mathbf{x}). \quad (44)$$

The first term in Eq. (44) is the contribution to total energy resulting from cell-cell and cell-medium adhesion. The second term allows deformation of cells with volume a_σ about a target volume (area in 2D space) A_σ, depending on the Potts parameters γ_τ. The target volume is twice that of the initial volume and it corresponds to the volume at which a cell undergoes mitosis, thereby creating a new cell. Thus cell proliferation is contemplated in this CPM. A variation of the last term in (44) is

$$\Delta H_{\text{chem}} = -\mu_\sigma [C(t,\mathbf{x}) - C(t,\mathbf{x}')], \quad (45)$$

where $\mathbf{x}$ and $\mathbf{x}'$ are two randomly picked neighboring lattice cells, $\mu_\sigma > 0$ is the chemical potential, and Eq. (45) represents chemotaxis favoring motion directed along the VEGF gradient. The VEGF concentration satisfies a reaction-diffusion equation [29]. The parameters appearing in the model are chosen in such a way that the progression of blood vessels occurs in the time scale observed in experiments [29].

Under this framework, each entity (ECs, ECM, ...) has a finite volume, a deformable shape and competes for space. ECs proliferate. Intercellular interactions occur only at the cells surface and have a cell-type-dependent surface (or adhesion) energy $J_{\tau,\tau'}$, which is a measure of the coupling strength between the entities τ and τ'. Other CPMs include an ECM strain-dependent term that favors cell extension in the direction of principal strain (durotaxis). The force exerted by the ECs on the ECM is calculated by finite elements [30]. In more complicated models, each cell contains agents that signal to other cells and adhesion is modeled by a CPM [31].

As in the case of random walk tip cell models, there is a connection between CPM and a deterministic formulation for a density. In [32], Alber *et al.* have written a discrete time master equation for the probability density $P(t,\mathbf{r},\mathbf{L})$ that a cell with its center of mass at $\mathbf{r}$ occupy a rectangle with sides $\mathbf{L} = (l_x, l_y)$ at time t. It is based on a CPM with energy given by (44), but with a target perimeter instead of the target area. The corresponding term in the energy is

$$H_{\text{perim}} = \sum_{\text{cells}} [\gamma_x (l_x - L_x)^2 + \gamma_y (l_y - L_y)^2]. \quad (46)$$

Here cells are always rectangles and do not proliferate nor die. Assuming that cells contain many lattice sites, they change little at each Monte Carlo step. Assuming further that cell-cell interactions are always binary, the authors derive a Fokker-Planck equation for $P(t, \mathbf{r}, \mathbf{L})$. These formulations would have to be extended to CPMs that include cell proliferation and be connected to mesoscopic angiogenesis models: from cell densities to densities of active vessel tip cells. It would be interesting to study whether the concept of active vessel tips and related ones can be used to derive deterministic descriptions in the spirit of Sects. 3 and 5.

7 Blood Flow and Vascular Network

Once a vascular network is being created, blood flows through the capillaries, anastomosis enhances flow in some of them and secondary angiogenesis may start in new vessels. Pries and coworkers have modeled blood flow in a vascular network and the response thereof to changing conditions such as pressure differences and wall stresses [33,34]. This response may remodel the vascular network by changing the radii of certain capillaries, and altering the distribution of blood flow [33,34]. McDougall, Anderson and Chaplain [35] have used this formulation to add secondary branching from new capillaries induced by wall shear stress to the original random walk tip cell model [13]. Blood flows according to Poiseuille's law, mass is conserved, there are empirical expressions for blood viscosity and for the wall shear stresses, and radii of capillaries adapt to local conditions. Secondary vessel branching may occur after the new vessel has reached a certain level of maturation and before a basal lamina has formed about it [21,35]. During such a time interval, the probability of secondary branching increases with both the local VEGF concentration and the magnitude of the shear stress affecting the vessel wall. McDougall *et al.*'s model can be used to figure out how drugs could be transported through the blood vessels and eventually reach a tumor [21,35]. In dense vessel networks, secondary branching may have little effect on the number of active tips at a given time, as anastomosis could eliminate secondary branches quickly. Thus we may ignore secondary branching when considering the density of active tips in such networks. Of course we cannot ignore it when describing blood flow and network remodeling.

One missing feature of angiogenesis models that take blood flow into account seems to be pruning. It is known that capillaries with insufficient blood circulation may atrophy and disappear. Pruning such blood vessels is an important mechanism to achieve a hierarchical vascular network such as that observed in retinal vascularization during development [3,4]. Global optimization and adaptation in developing networks has been recently shown to lead to highly optimized transport vascular systems [36,37]. It would be interesting to adapt these studies to angiogenesis.

8 Phase Field Models

Phase field models are continuum models able to represent vascular networks. For example, Travasso et al. [39,40] consider a reaction-diffusion equation for the VEGF $C(t,\mathbf{x})$ coupled to a continuum equation for the phase field $\phi(t,\mathbf{x})$:

$$\frac{\partial C}{\partial t}(t,\mathbf{x}) = \kappa_c \Delta_x C(t,\mathbf{x}) - \chi_c C(t,\mathbf{x})\,\phi(t,\mathbf{x})\,\Theta(\phi(t,\mathbf{x})), \tag{47}$$

$$\frac{\partial \phi}{\partial t}(t,\mathbf{x}) = M\Delta_x[-\phi(t,\mathbf{x}) + \phi^3(t,\mathbf{x}) - \varepsilon^2\Delta_x\phi(t,\mathbf{x})] + \alpha_\phi(C(t,\mathbf{x}))\,\phi(t,\mathbf{x})\,\Theta(\phi(t,\mathbf{x})). \tag{48}$$

Here M is the mobility coefficient for the endothelial cells, the proliferation rate is $\alpha_\phi(C) = \alpha_\phi[C\Theta(C_p - C) + C_p\Theta(C - C_p)]$, ε is the width of the capillary wall, and $\Theta(x)$ is the Heaviside unit step function. Proliferative and non-activated cells are described by an order parameter ϕ which is equal to -1 at the ECM outside the capillary and $+1$ inside it. Areas of high proliferation of endothelial cells have $\phi > 1$, which will lead to the widening of the capillary. The position of the capillary wall made out of stalk cells is given by the level set $\phi(t,\mathbf{x}) = 0$.

In addition to the continuum equations, there are discrete equations for activated tip endothelial cells and criteria to distinguish them. The angiogenic factor at the tip cell is only consumed at its surface receptors, therefore $\chi_C = 0$ is set in Eq. (47) at all points inside the tip cell. A tip cell moves chemotactically with velocity $\mathbf{v}$ (proportional to the VEGF gradient $\nabla_x C$ measured at the tip cell center, $\mathbf{x}_t(t)$):

$$\mathbf{v}(\mathbf{x}_t(t)) = \chi_v(|\nabla_x C(t,\mathbf{x_t})|)\,\nabla_x C(t,\mathbf{x}_t), \tag{49}$$

$$\chi_v(g) = \chi_v\left[\Theta(g - g_m) + \left(\frac{g_M}{g} - 1\right)\Theta(g - g_M)\right], \tag{50}$$

where χ_v is the chemotactic response of the endothelial cells (having radius R_c), g_M is the maximum VEGF gradient and $\chi_v g_M$ is the maximum tip speed. An activated cell moves only if $g_m < |\nabla_x C(t,\mathbf{x}_t)|$, with $0 < g_m < g_M$. When these conditions are met at the center of an endothelial stalk cell and $C > C_c$ there, it acquires the tip cell phenotype, with the caveat that cell-cell contact dependent mechanisms (the Notch pathway) prevent the activation of two neighboring cells. Only points for which there is a minimum distance of $4R_c$ to the centers of all already existing tip cells can become centers of activated tip cells. As in the biological system, when the chemotactic signal is small, $C < C_c$ or $|\nabla_x C(t,\mathbf{x}_t)| < g_m$, the endothelial cell returns to the stalk cell state. Simulations show that tip cell velocity and stalk cell proliferation play important roles in vascular network morphology [39]. An increase in stalk cell proliferation leads to a more branched network constituted by thicker vessels, while a higher tip cell migration velocity leads to a more branched network with thinner vessels [39].

More general phase field models incorporate force at the vessel tip and elasticity [38] and haptotaxis [41]. They are included in the review paper [42].

A study of the relation between morphology of the blood vessel network generated by phase field models, blood supply and obstructions can be found in [43]. Phase field models are thus a deterministic alternative to stochastic models.

9 Conclusions

Angiogenesis is a complex multiscale process by which diffusing vessel endothelial growth factors induce sprouting of blood vessels that carry oxygen and nutrients to hypoxic tissue. Cancerous tumor cells profit from this process to prosper, grow and eventually migrate to other organs. Mathematical models contemplate different aspects of angiogenesis. Here we have reviewed recent work on a simple tip cell model that encompasses vessel extension driven by chemotaxis and described by Langevin equations, stochastic tip branching and vessel fusion (anastomosis). From the stochastic description, we have derived a deterministic integropartial differential equation for the density of active tip cells coupled with a reaction-diffusion equation for the growth factor. The associated initial-boundary value problem is well posed. It is important to note that anastomosis prevents proliferation of active tips and therefore the deterministic description is based on ensemble averages over replicas of the stochastic process. Numerical simulations of both (deterministic and stochastic) descriptions show that the density of active tips adopts the shape of a two-dimensional soliton-like wave (angiton) after a formation stage. We have found an analytical formula for the one-dimensional projection of the soliton and ordinary differential equations for variables that provide its velocity, position and size. These equations also characterize the advance of the vessel network for single replicas. Much more work needs to be carried out to solve mathematical issues arising from our results, both from analysis of the deterministic description and from establishing more precise conditions for its validity. The description of the soliton should be extended to the true two-dimensional soliton (angiton) that appears in the numerical simulations and to the case of a more general geometry than that of the slab. Fluctuations cannot be ignored in the case of ensemble averages, and future work predicting the evolution of a real vessel network should include confidence bands about averages. Anti-angiogenic treatments need to be improved [1,2], and, in this respect, having better models and theories about their solutions should help. Therapies are related to optimal control of angiogenesis and they require accurate mathematical models, validated by comparison with real data (inverse problems - statistics of random geometric structures).

We have also related the specific model we study to other tip cells models in the literature that describe vessel extension by reinforced random walks instead of stochastic differential equations. Our methodology may be adapted to these other models as Langevin equations arise from reinforced random walks in appropriate limits. All these models describe mesoscales in which cells are just point particles, thereby ignoring their shapes and a microscopic description thereof. Other models consider the evolution of individual endothelial cells of variable shape and extension through cellular Potts models, but the continuation of these

models toward the mesoscale has barely begun. Extending the analysis carried out for our mesoscopic stochastic tip cell model to microscopic models is a challenge for the future. Blood circulation through the angiogenic network favors certain vessels, others that do not have enough perfusion shrink and disappear and secondary branching may occur. Future work could delve deeper in the topics of vessel remodeling, pruning, formation of optimal vascular networks and transport of medicals through them.

Apart from the specific application to angiogenesis, we have presented in this paper methodological contributions for a sound mathematical modeling of stochastic vessel networks: (a) the use of stochastic distributions, and their mean densities, describing the vessels, which are random objects of Hausdorff dimension one, cf (7); (b) reduction of vessel distributions to integrals over time of active tip distributions, which are random objects of zero Hausdorff dimension, cf (8)–(10); (c) characterization of the attractor of the density of active tips as a soliton whose position, velocity and size are given as solutions of ordinary differential equations, cf (17), (23)–(24). In our system, which is strongly out of equilibrium, this attractor plays a similar role to the stable stationary equilibrium distribution of many physical systems.

Acknowledgements. The authors thank V. Capasso and D. Morale from the Department of Mathematics of Università degli Studi di Milano, Milan, Italy, and B. Birnir from the Department of Mathematics of University of California at Santa Barbara, USA, for fruitful discussions and contributions. We also thank A. Lasanta from Universidad Carlos III de Madrid for useful comments on the manuscript. This work has been supported by the Ministerio de Economía y Competitividad grants MTM2014-56948-C2-2-P and MTM2017-84446-C2-2-R.

References

1. Carmeliet, P.F.: Angiogenesis in life, disease and medicine. Nature **438**, 932–936 (2005)
2. Carmeliet, P., Jain, R.K.: Molecular mechanisms and clinical applications of angiogenesis. Nature **473**, 298–307 (2011)
3. Gariano, R.F., Gardner, T.W.: Retinal angiogenesis in development and disease. Nature **438**, 960–966 (2005)
4. Fruttiger, M.: Development of the retinal vasculature. Angiogenesis **10**, 77–88 (2007)
5. Carmeliet, P., Tessier-Lavigne, M.: Common mechanisms of nerve and blood vessel wiring. Nature **436**, 193–200 (2005)
6. Folkman, J.: Tumor angiogenesis: therapeutic implications. N. Engl. J. Med. **285**(21), 1182–1186 (1971)
7. Folkman, J.: Angiogenesis. Annu. Rev. Med. **57**, 1–18 (2006)
8. Heck, T., Vaeyens, M.M., Van Oosterwyck, H.: Computational models of sprouting angiogenesis and cell migration: towards multiscale mechanochemical models of angiogenesis. Math. Model. Nat. Phen. **10**, 108–141 (2015)
9. Bonilla, L.L., Capasso, V., Alvaro, M., Carretero, M.: Hybrid modeling of tumor-induced angiogenesis. Phys. Rev. E **90**, 062716 (2014)

10. Terragni, F., Carretero, M., Capasso, V., Bonilla, L.L.: Stochastic model of tumor-induced angiogenesis: ensemble averages and deterministic equations. Phys. Rev. E **93**, 022413 (2016)
11. Bonilla, L.L., Carretero, M., Terragni, F., Birnir, B.: Soliton driven angiogenesis. Sci. Rep. **6**, 31296 (2016)
12. Bonilla, L.L., Carretero, M., Terragni, F.: Solitonlike attractor for blood vessel tip density in angiogenesis. Phys. Rev. E **94**, 062415 (2016)
13. Anderson, A.R.A., Chaplain, M.A.J.: Continuous and discrete mathematical models of tumor-induced angiogenesis. Bull. Math. Biol. **60**, 857–900 (1998)
14. Plank, M.J., Sleeman, B.D.: Lattice and non-lattice models of tumour angiogenesis. Bull. Math. Biol. **66**, 1785–1819 (2004)
15. Stokes, C.L., Lauffenburger, D.A.: Analysis of the roles of microvessel endothelial cell random motility and chemotaxis in angiogenesis. J. Theor. Biol. **152**, 377–403 (1991)
16. Stokes, C.L., Lauffenburger, D.A., Williams, S.K.: Migration of individual microvessel endothelial cells: stochastic model and parameter measurement. J. Cell Sci. **99**, 419–430 (1991)
17. Capasso, V., Morale, D.: Stochastic modelling of tumour-induced angiogenesis. J. Math. Biol. **58**, 219–233 (2009)
18. Sun, S., Wheeler, M.F., Obeyesekere, M., Patrick Jr., C.W.: Multiscale angiogenesis modeling using mixed finite element methods. Multiscale Mod. Simul. **4**(4), 1137–1167 (2005)
19. Bonilla, L.L., Capasso, V., Alvaro, M., Carretero, M., Terragni, F.: On the mathematical modelling of tumour induced driven angiogenesis. Math. Biosci. Eng. **14**, 45–66 (2017)
20. Bonilla, L.L., Carretero, M., Terragni, F.: Ensemble averages, soliton dynamics and influence of haptotaxis in a model of tumor-induced angiogenesis. Entropy **19**, 209 (2017)
21. Stéphanou, A., McDougall, S.R., Anderson, A.R.A., Chaplain, M.A.J.: Mathematical modelling of the influence of blood rheological properties upon adaptative tumour-induced angiogenesis. Math. Comput. Model. **44**, 96–123 (2006)
22. Gardiner, C.W.: Stochastic Methods. A Handbook for the Natural and Social Sciences, 4th edn. Springer, Berlin (2010)
23. Carpio, A., Duro, G.: Well posedness of an angiogenesis related integrodifferential diffusion model. Appl. Math. Model. **40**, 5560–5575 (2016)
24. Carpio, A., Duro, G., Negreanu, M.: Constructing solutions for a kinetic model of angiogenesis in annular domains. Appl. Math. Model. **45**, 303–322 (2017)
25. Capasso, V., Flandoli, F.: On the mean field approximation of a stochastic model of tumor-induced angiogenesis. Eur. J. Appl. Math. (2018). https://doi.org/10.1017/S0956792518000347
26. Levine, H.A., Pamuk, S., Sleeman, B.D., Nilsen-Hamilton, M.: Mathematical modeling of the capillary formation and development in tumor angiogenesis: penetration into the stroma. Bull. Math. Biol. **63**, 801–863 (2001)
27. Hill, N.A., Häder, D.P.: A biased random walk model for the trajectories of swimming micro-organisms. J. Theor. Biol. **186**, 503–526 (1997)
28. Bonilla, L.L., Carretero, M., Terragni, F.: Integrodifference master equation describing actively growing blood vessels in angiogenesis. Preprint (2019)
29. Bauer, A.L., Jackson, T.L., Jiang, Y.: A cell-based model exhibiting branching and anastomosis during tumor-induced angiogenesis. Biophys. J. **92**, 3105–3121 (2007)

30. Van Oers, R.F.M., Rens, E.G., La Valley, D.J., Reinhart-King, C.A., Merks, R.M.H.: Mechanical cell-matrix feedback explains pairwise and collective endothelial cell behavior in vitro. PLoS Comput. Biol. **10**(8), el003774 (2014)
31. Bentley, K., Franco, C.A., Philippides, A., Blanco, R., Dierkes, M., Gebala, V., Stanchi, F., Jones, M., Aspalter, I.M., Cagna, G., Weström, S., Claesson-Welsh, L., Vestweber, D., Gerhardt, H.: The role of differential VE-cadherin dynamics in cell rearrangement during angiogenesis. Nat. Cell Biol. **16**(4), 309–321 (2014)
32. Alber, N., Chen, N., Lushnikov, P.M., Newman, S.A.: Continuous macroscopic limit of a discrete stochastic model for interaction of living cells. Phys. Rev. Lett. **99**, 168102 (2007)
33. Pries, A.R., Secomb, T.W., Gaehtgens, P.: Structural adaptation and stability of microvascular netwoks: theory and simulation. Am. J. Physiol. Heart Circ. Physiol. **275**(44), H349–H360 (1998)
34. Pries, A.R., Secomb, T.W.: Control of blood vessel structure: insights from theoretical models. Am. J. Physiol. Heart Circ. Physiol. **288**(3), H1010–H1015 (2005)
35. McDougall, S.R., Anderson, A.R.A., Chaplain, M.A.J.: Mathematical modelling of dynamic adaptive tumour-induced angiogenesis: clinical implications and therapeutic targeting strategies. J. Theor. Biol. **241**, 564–589 (2006)
36. Ronellenfitsch, H., Katifori, E.: Global optimization, local adaptation, and the role of growth in distribution networks. Phys. Rev. Lett. **117**, 138301 (2016)
37. Ronellenfitsch, H., Lasser, J., Daly, D.C., Katifori, E.: Topological phenotypes constitute a new dimension in the phenotypic space of leaf venation networks. PLOS Comput. Biol. **11**(12), e1004680 (2016)
38. Santos-Oliveira, P., Correia, A., Rodrigues, T., Ribeiro-Rodrigues, T.M., Matafome, P., Rodríguez-Manzaneque, J.C., Seią, R., Girão, H., Travasso, R.D.M.: The force at the tip - modelling tension and proliferation in sprouting angiogenesis. PLoS Comput. Biol. **11**(8), e1004436 (2015)
39. Travasso, R.D.M., Corvera Poiré, E., Castro, M., Rodríguez-Manzaneque, J.C., Hernández-Machado, A.: Tumor angiogenesis and vascular patterning: a mathematical model. PLoS ONE **6**(5), e19989 (2011)
40. Travasso, R.D.M., Castro, M., Oliveira, J.C.R.E.: The phase-field model in tumor growth. Phil. Mag. **91**(1), 183–206 (2011)
41. Vilanova, G., Colominas, I., Gomez, H.: Coupling of discrete random walks and continuous modeling for three-dimensional tumor-induced angiogenesis. Comput. Mech. **53**, 449–464 (2014)
42. Vilanova, G., Colominas, I., Gomez, H.: Computational modeling of tumor-induced angiogenesis. Arch. Computat. Methods Eng. **24**, 1071–1102 (2017)
43. Torres-Rojas, A., Meza Romero, A., Pagonabarraga, I., Travasso, R.D.M., Corvera Poiré, E.: Obstructions in vascular networks. critical vs non-critical topological sites for blood supply. PLoS ONE **10**, e0128111 (2015)